minerals

MDPI

Article

Supergene Uranyl Mineralization of the Rabejac Deposit, Lodève, France

Fabrice Dal Bo [1,*], Frédéric Hatert [1] and Simon Philippo [2]

[1] Laboratoire de Minéralogie, B18, Université de Liège, 4000 Liège, Belgium; fhatert@uliege.be
[2] Section Minéralogie, Musée d'Histoire Naturelle, Rue Münster 25, 2160 Luxembourg, Luxembourg; simon.philippo@mnhn.lu
* Correspondence: fabrice.dalbo@gmail.com

Received: 21 August 2018; Accepted: 11 September 2018; Published: 18 September 2018

Abstract: The Rabejac uranium deposit that is located in the Lodève region, France, is the type locality for three uranyl minerals species (fontanite, seelite, and rabejacite). In addition, this deposit shows an extraordinary supergene uranyl mineralization characterized by the presence of many rare secondary uranyl species. In the present study, a mineralogical description as well as new chemical and crystallographic data are reported on (meta)zeunerite, (meta)nováčekite, (meta)uranospinite, heinrichite, nováčekite-I, arsenuranospathite, umohoite, calcurmolite, becquerelite, billietite, and liebigite. The chemical data indicate that the arsenate members of the autunite/meta-autunite group incorporate a significant amount of phosphorus. Moreover, the uranospinite samples usually exhibit high Mg content, thus moving toward the nováčekite end-member composition. The refined unit-cell parameters for all of the investigated mineral species are in agreement with the previous data reported in the literature. Finally, a model describing the alteration of the primary uraninite and the formation of secondary uranyl minerals is proposed in agreement with the observed mineral assemblages.

Keywords: uranyl minerals; autunite group; EMPA; single-crystal X-ray; crystal structure; mineral evolution

1. Introduction

Since 1960, the number of described uranyl mineral species has been multiplied by three, and to date, more than 250 mineral species containing uranium as a main structural element are reported in nature. This tendency is still going on and many novel uranyl minerals showing novel chemical compositions and structural arrangements are still reported each year. The most remarkable and recent discovery is certainly ewingite, $Mg_8Ca_8(UO_2)_{24}(CO_3)_{30}O_4(OH)_{12}(H_2O)_{138}$, the most structurally complex mineral [1]. Based on unexampled nanoscale uranyl carbonate cages, the crystal structure of ewingite emphasizes how uranyl carbonate minerals are important in the control of the mobility of uranium in groundwater under neutral and alkaline conditions. In addition, this discovery highlights that the study of the alteration processes of uraninite, as well as the intermediate and final products of these processes, are crucial for the understanding of the evolution of used nuclear fuel in the case of long-term disposal in geological repositories.

The Rabejac deposit has provided very interesting samples to study the weathering of primary uraninite and the formation of secondary uranyl minerals. The mineralogical associations that were observed in Rabejac are common with those observed in the other uranium mines of the Lodève basin. However, the Rabejac mine contains in addition rare species, such as uranyl arsenates and uranyl molybdates. The Rabejac mine is also the type locality for three uranyl mineral species: fontanite $Ca[(UO_2)_3O_2(CO_3)_2](H_2O)_6$ [2,3], seelite $Mg[(UO_2)_2(As^{3+}O_3)_2](H_2O)_7$ [4,5], and rabejacite $Ca_2[(UO_2)_4O_4(SO_4)_2](H_2O)_8$ [6,7].

The mining history of the Lodève uranium deposits started in 1957 with the discovery of a radiometric anomaly in the locality of Rabejac. However, the first mining investigations in the area, one shaft of 27 m and 156 m of galleries gave a disappointing estimation of the volume of uranium ore [8]. During the following year, more surface radiometric anomalies were detected in the areas of Mas d'Alary, Riviéral, Les Mares, Usclas, and Le Puech. In 1959, new underground-prospecting works in the Rabejac and Mas d'Alary deposits reveal a potential of 1300 and 2000 tons of uranium, respectively. In 1962, 800 m of galleries and one shaft of 27 m are already dug in Mas d'Alary in order to start the mining exploitation, as well as the construction of one refinement factory in Forez. In the seventies, due to the first oil crisis and the huge increase of the oil price, the French government decided to build new nuclear stations. In order to supply these new reactors with nuclear fuel the prospections in the Lodève basin were heightened and the global potential of the deposits was estimated to be 20,000 tons of uranium. At the beginning of 1976, the COGEMA (Compagnie Générale des Matières Nucléaires) company is created to control the mining operations, and the production peak is reached in 1983 with more than 1032 tons of uranium refined. From 1988 the exchange rates of uranium slumped and the production rate of the Lodève mines was decreased. In 1993, the COGEMA group reduced the workforce by half, and the production rate was decreased from 950 tons to 500 tons of uranium per year. The mining activities were definitively shut down in 1997, the refinement factories were dismantled, and the mining sites were restored. In total, the Lodève mines have produced more than 14,000 tons of uranium [9]. The Rabejac deposit was mined between 1989 and 1992, and it provided around 40 tons of uranium.

In the present study we report a mineralogical description as well as new chemical and crystallographic data for the following mineral species: (meta)zeunerite, (meta)nováčekite, (meta)uranospinite, heinrichite, nováčekite-I, arsenuranospathite, umohoite, calcurmolite, becquerelite, billietite, and liebigite. In addition, a description of the alteration of the primary uraninite and of the formation of secondary uranyl minerals is proposed in agreement with the observed mineral assemblages.

2. Geological Setting

The Rabejac deposit is located in the Permian Lodève basin that is limited by the locality of Lodève, Saint-Privas, Clermont-l'Hérault, La Tour-sur-Orb, and Lumas. The Lodève basin is a geomorphological unit that is located in the south of the Central Massif, France (Figure 1). This basin has a surface area of 25 × 10 km^2 and is surrounded by the Black Mountain in the north, the Causses of Larzac in the north and north-east, and the plains of Languedoc in the south-east.

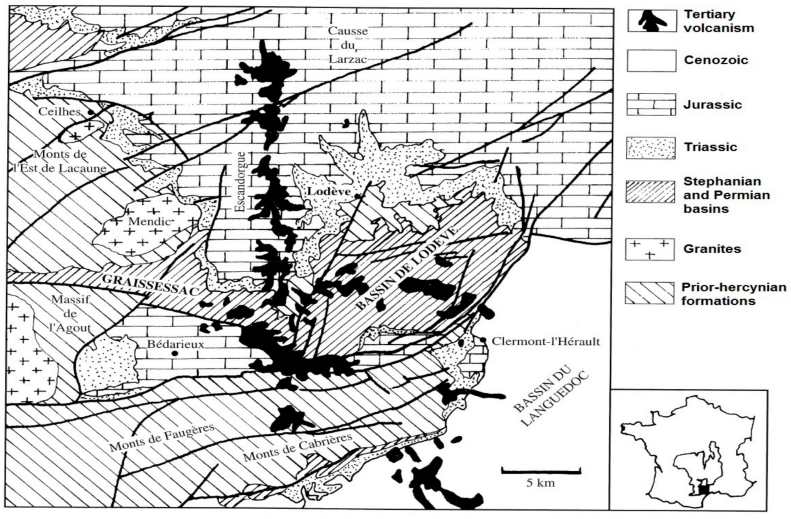

Figure 1. Geographical situation of the Permian Lodève basin (modified from Caubel, 1997 [10]).

The main geological feature of the Lodève basin is described as a monoclinal structure tilted 15° to the south. The base of the basin is constituted by Cambrian dolomite, which is covered by Stephanian and Permian rocks [11]. The Permian record is about 2500 m and is divided into three series: the Autunian (160–240 m) and Saxonian (200 m) series constituted by a succession of grey sandstones, siltstones, arenites, and organic matter-bearing carbonate shales; and, the Thuringian series (2000 m) characterized by sandstones and pyrite-bearing schists [8]. The Thuringian typically contains several white ash layers (5 to 50 cm). The Permian deposits are highly faulted by several orogenic phases, and the faults that were formed by these tectonic events have contributed to the remobilization of the uranium during the Lias, Aptian-Albian, Oligocene, and Miocene periods [8,12].

The Rabejac deposit is the only one located in the Thuringian series, while all the other uranium mines are located in the Autunian and Saxonian series (Figure 2). The uranium mineralization generally occurs as fracture fillings and around the fault zones crossing the Thuringian series. The uranium ore also occurs as metrical stratiform lens and plurimetrical massive uraninite (variety pitchblende) near the surface, giving the Rabejac deposit a very high uranium concentration [6,8,10].

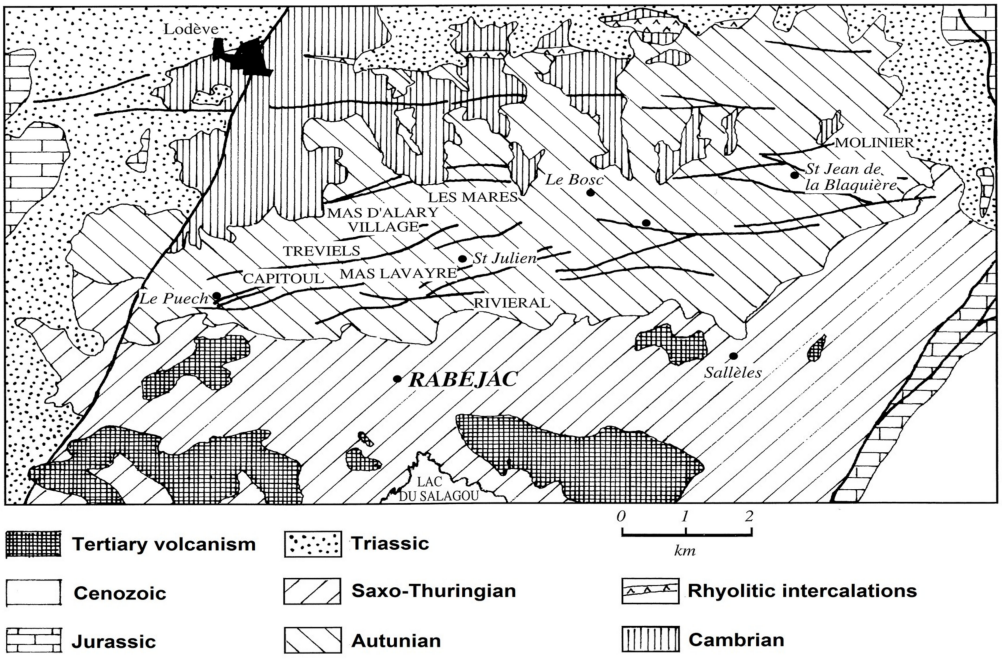

Figure 2. Geological map of the Permian Lodève basin, showing the geographical localization of the uranium mines (modified from Caubel, 1997 [10]).

3. Materials and Methods

All of the mineral samples studied in this work are from the collections of the National Museum of Natural History of Luxembourg. The mineral collector Alain Caubel left the samples to the Museum. In total, more than fifty minerals samples containing uranium have been investigated.

3.1. Powder X-ray Diffration (PXRD)

The powder X-ray diffraction technique was used for the identification of mineral species. Identification was performed by comparison between the collected powder X-ray diffraction patterns and the data from the International Centre for Diffraction Data (ICDD). Several diffractometers were used: Malvern-Panalytical PW 3710 (Worcestershire, UK) (FeK_α radiation; λ = 1.9373 Å), Bruker D8 Advance ECO (Billerica, MA, USA) (CuK_α radiation; λ = 1.54178 Å) and Rigaku Oxford Diffraction Xcalibur four-circle (Oxford, UK) (MoK_α radiation, λ = 0.71073 Å). In the case of very low amount of material being available, the measurements were performed on a four-circle diffractometer used in a Debye-Scherrer-type scan mode. In order to refine the unit-cell parameters from powder

X-ray diffraction, the values of the diffraction peaks (*d*) were corrected with an internal standard ($Pb(NO_3)_2$). The parameters were calculated while using the least-squares refinement software LCLSQ in version 8.4 [13]. The unit-cell parameters were refined using the CrysAlisRED package [14].

3.2. Single-Crystal X-ray Diffraction (SXRD)

Single-crystal X-ray studies were carried out on an Rigaku Oxford Diffraction Xcalibur four-circle diffractometer (kappa geometry, Oxford, UK), using the MoK_α radiation (λ = 0.71073 Å, 40 kV, 40 mA), and equipped with an EOS CCD area detector. The unit-cell parameters were refined while using the CrysAlisRED package [14]. In the case of structure refinement the data were corrected for Lorentz, polarization and absorption effects, the latter with an empirical method using the SCALE3 ABSPACK scaling algorithm included in the CrysAlisRED package [14]. The crystal structure of becquerelite, billietite, and liebigite were solved by direct methods and subsequently refined while using SHELXS and SHELXL softwares [15]. Scattering curves for neutral atoms and anomalous dispersion correction were taken from the International Tables for X-ray Crystallography, Vol. C [16].

Bond valence theory was used to confirm the oxidation state of cations, to make the distinction between O^{2-}, OH^-, and H_2O groups, and to support the validity of the structural results. The bond-valence sums (BVS) were calculated using the parameters of Brown and Altermatt (1985) [17] and of Burns et al. (1997) for U^{6+} [18].

As these new structural refinements are in complete agreement with the previous one reported in the literature, the description of the crystal structures and the new data collected for becquerelite, billietite, and liebigite are provided in the Supplementary Materials section of this manuscript.

3.3. Electron Probe Microanalysis (EPMA)

Quantitative chemical analyses were performed with a Cameca SX-100 electron probe micro-analyzer (Laboratoire Magmas et Volcans, Université Blaise Plascal, Clermont-Ferrand, France) operating in the wavelength-dispersion mode, with an accelerating voltage of 15 kV, a beam current of 2 nA, and a beam diameter of 20 µm. The beam diameter was sometimes reduced to 10 µm when the sample was able to support the heat from the electron beam. Attempts to use a beam current of 5 nA were made, but they lead to the destruction of the sample. The following standards and lines were used: GaAs (AsL_α); Al_2O_3 (AlK_α); UO_2 (UM_β); $CaMoO_4$ (MoL_α); $BaSO_4$ (SK_α, BaL_α); apatite (PK_α, CaK_α); chalcopyrite (CuK_α); fayalite (FeK_α); albite (NaK_α); MgO (MgK_α); CaF_2 (FK_α); and, wollastonite (SiK_α). Fluorine was analyzed only for the arsenuranospathite samples. Counting time was 10–20 s on peak depending on the element, and 50% of that time for the background. Water content was calculated by stoichiometry from the results of the crystal-structure analyses or according to the theoretical chemical formula of the mineral. Elevated analytical totals can be accounted for water evaporation due to the high vacuum or to the heating of the area analysed by the electron beam. Despite the use of a low beam current and a large beam diameter, this phenomenon is quite common with minerals containing a very large amount of structural water. Minerals of the autunite and meta-autunite group are especially very sensitive to this phenomenon. The mentions *apfu* and *pfu* in the text and tables mean *atom per formula unit* and *per formula unit*, respectively. The number *n* in the Tables indicates the number of point analyses performed on one sample.

4. Mineralogical and Chemical Description of the Uranyl Minerals

4.1. Minerals of the Autunite and Meta-Autunite Group

4.1.1. Zeunerite/Metazeunerite—$Cu[(UO_2)(AsO_4)]_2(H_2O)_{12\text{-}8}$

Both zeunerite and metazeunerite are usually well crystallized and they form tetragonal crystals tabular on {001}. The crystals are often associated in subparallel growths, up to several millimeters across. Zeunerite crystals are transparent and emerald-green, while metazeunerite crystals are

translucent with a darker green color. However, these observations are not sufficient to distinguish hydrated zeunerite from its dehydrated analogue; when they are thick, some zeunerite crystals become dark-green and dull. In addition to the basal cleavage on (001), a perfect cleavage plane is observed along (100). Zeunerite and metazeunerite are often observed in association with other arsenates of the autunite group, and also with uranophane-α. Less frequently, these copper uranyl minerals are also occurring in association with vandendriesscheite, rutherfordine, and sklodowskite, and also with copper uranium-free minerals, such as cornwallite, tyrolite, malachite, and cuprite.

With the exception of sample U008, chemical analyses on zeunerite and metazeunerite from Rabejac indicate that Cu is practically never substituted by any other cation (0.86–1.01 *apfu*, Tables 1 and 2). In all analyses, the cationic total for the interstitial site (*A*) remains close to 1 (0.97 to 1.09 *apfu*). However, the isomorphism in the zeunerite-torbernite series is well established with a variation of the $(AsO_4)^{3-}$ anionic group content from 1.97 to 1.06 *apfu*, while the $(PO_4)^{3-}$ anionic group content varies between 0.93 and 0.02 *apfu* (Figure 3). In all samples, the U content is very close to 2 *apfu*. The chemical formulae of the extreme members of this series observed in Rabejac are given by $(Cu_{0.97}Na_{0.01})_{\sum 0.98}[(U_{1.04}O_2)(As_{0.99}P_{0.01}O_4)]_2(H_2O)_{12}$ and $Cu_{0.97}[(U_{1.00}O_2)(As_{0.53}P_{0.47}O_4)]_2(H_2O)_{10}$. In all samples except VC2164, the $(SO_4)^{2-}$ and $(SiO_4)^{4-}$ anionic groups are very low (<0.02 *apfu*). In VC2164, the close association of uranophane-α with metazeunerite crystals may explain the high $(SiO_4)^{4-}$ anionic group contents (0.12 *apfu*).

Table 1. Chemical composition of zeunerite.

Sample	U025	U019	VC2159	VC2135	U030	VC2144	VC2165
n	8	7	10	10	8	9	8
SO_3 wt %	0.03	0.12	0.05	0.08	0.09	0.03	0.02
SiO_2	0.02	0.05	0.03	0.02	0.01	0.02	0.01
As_2O_5	22.43	21.24	18.29	21.64	13.72	22.40	21.57
P_2O_5	0.44	1.20	3.32	1.76	7.01	0.19	0.24
Al_2O_3	0.02	0.01	0.02	0.00	0.01	0.02	0.01
CuO	7.91	7.80	7.89	8.18	8.57	7.99	7.73
FeO	0.07	0.07	0.02	0.17	0.03	0.03	0.03
MgO	0.05	0.00	0.02	0.02	0.02	0.02	0.02
CaO	0.06	0.07	0.04	0.04	0.06	0.04	0.03
BaO	0.07	0.07	0.13	0.01	0.18	0.05	0.12
Na_2O	0.04	0.04	0.04	0.00	0.03	0.00	0.05
UO_3	60.40	58.29	60.58	61.94	62.46	58.46	57.94
H_2O	10.92	11.03	11.19	11.59	11.86	10.72	10.35
Total	102.46	99.99	101.62	105.45	104.05	99.97	98.12
Cation numbers based on As + P + Si + S = 2 *apfu*							
S^{6+}	0.003	0.015	0.006	0.009	0.010	0.004	0.003
Si	0.004	0.008	0.005	0.003	0.002	0.003	0.002
As	1.932	1.811	1.537	1.756	1.088	1.966	1.960
P	0.061	0.166	0.452	0.231	0.900	0.027	0.035
Σ*T* site	2.000	2.000	2.000	2.000	2.000	2.000	2.000
Al	0.004	0.002	0.004	0.000	0.002	0.004	0.002
Cu	0.984	0.961	0.958	0.959	0.982	1.013	1.015
Fe^{2+}	0.010	0.010	0.003	0.022	0.004	0.004	0.004
Mg	0.012	0.000	0.005	0.005	0.005	0.005	0.005
Ca	0.011	0.012	0.007	0.007	0.010	0.007	0.006
Ba	0.005	0.004	0.008	0.001	0.011	0.003	0.008
Na	0.013	0.013	0.012	0.000	0.009	0.000	0.017
Σ*A* site	1.039	1.002	0.997	0.994	1.023	1.036	1.057
U^{6+}	2.090	1.997	2.046	2.020	1.990	2.061	2.116
H_2O	12	12	12	12	12	12	12

Table 2. Chemical composition of metazeunerite.

Sample	U008	U040	U009	VC2139	U008 *	U029	VC2164
n	7	10	11	5	5	7	2
SO_3 wt %	0.03	0.06	0.06	0.08	0.01	0.06	0.03
SiO_2	0.04	0.04	0.06	0.03	0.08	0.00	0.78
As_2O_5	21.90	13.21	13.34	21.27	21.32	16.25	18.59
P_2O_5	0.11	7.18	7.05	0.50	1.37	4.86	2.44
Al_2O_3	0.01	0.04	0.01	0.01	0.02	0.01	0.19
CuO	7.44	8.37	8.21	7.71	4.23	8.20	7.20
FeO	0.05	0.04	0.05	0.03	0.09	0.04	0.05
MgO	0.01	0.02	0.01	0.07	0.32	0.03	0.03
CaO	0.04	0.04	0.02	0.17	2.36	0.05	0.13
BaO	0.07	0.11	0.13	0.20	0.34	0.00	0.46
Na_2O	0.03	0.03	0.01	0.06	0.04	0.01	0.05
UO_3	57.78	62.41	60.81	59.65	62.15	59.25	59.72
H_2O	6.96	7.84	7.82	6.98	7.42	7.59	7.55
Total	94.48	99.29	97.58	96.76	99.75	96.35	97.22
Cation numbers based on As + P + Si + S = 2 *apfu*							
S^{6+}	0.004	0.006	0.009	0.010	0.010	0.007	0.004
Si	0.007	0.007	0.009	0.005	0.002	0.000	0.124
As	1.973	1.057	1.075	1.912	1.801	1.343	1.544
P	0.016	0.930	0.907	0.073	0.187	0.650	0.328
Σ*T* site	2.000	2.000	2.000	2.000	2.000	2.000	2.000
Al	0.002	0.007	0.002	0.002	0.004	0.002	0.036
Cu	0.968	0.968	0.951	1.001	0.516	0.979	0.864
Fe^{2+}	0.007	0.005	0.006	0.004	0.012	0.005	0.007
Mg	0.003	0.005	0.002	0.018	0.077	0.007	0.007
Ca	0.007	0.007	0.003	0.031	0.409	0.008	0.022
Ba	0.005	0.001	0.008	0.013	0.022	0.000	0.029
Na	0.010	0.009	0.002	0.020	0.013	0.003	0.015
Σ*A* site	1.002	1.002	0.974	1.089	1.053	1.004	0.980
U^{6+}	2.091	2.006	1.958	2.154	2.110	1.967	1.993
H_2O	8	8	8	8	8	8	8

* Chemical analyses performed on yellowish crystals initially identified as uranospinite.

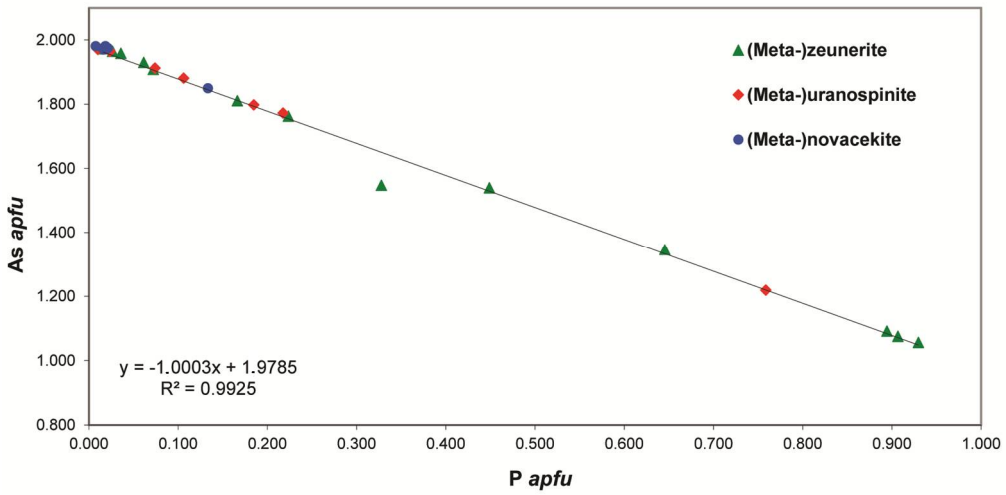

Figure 3. Binary plot of the As content versus the P content of Cu-, Ca-, and Mg-bearing arsenates members of the (meta-)autunite group from Rabejac.

The sample U008 contains three autunite-type uranyl arsenates: nováčekite, uranospinite, and metazeunerite. Chemical analyses performed on metazeunerite crystals indicate that the composition of this sample is very close to the composition of the As end-member of the zeunerite-torbernite series. At the opposite, chemical analyses performed on several yellow crystals from the same sample indicate that Cu is dominant on the *A* site (0.52 *apfu*), but accompanied by an unusual high amount of Ca (0.41 *apfu*). This sample also contains the highest amount of Mg (0.08 *apfu*) recorded for metazeunerite from Rabejac. The chemical formula of this specific sample is given by $(Cu_{0.52}Ca_{0.41}Mg_{0.08})_{\sum 1.01}[(U_{1.05}O_2)(As_{0.90}P_{0.10}O_4)]_2(H_2O)_8$. Ca-rich torbernite (up to 0.30 Ca *apfu*) is reported from Medvědín deposit, Czech Republic [19]. However, the replacement of Cu by Ca in the strongly distorted octahedral site (Jahn-Teller distortion), occurring in the structure of zeunerite-torbernite, is difficult to explain through crystallographic arguments. Therefore, it is likely that this specific chemical composition is the result of an intimate intergrowth of platy crystals of zeunerite and uranospinite.

Unit-cell parameters for zeunerite and metazeunerite, refined from single-crystal X-ray diffraction data (SXRD), are provided in Table 3. These parameters are in good agreement with those that are reported for natural samples [19] and for synthetic analogues [20]. A discrepancy is observed between the *c* unit-cell parameter measured on natural samples obtained in this work ($c \approx 8.70$ Å), and the doubled *c* parameter ($c \approx 17.42$ Å) usually reported for metazeunerite [21]. However, this lower *c* unit-cell parameter is in agreement with that reported by Hennig et al. (2003) [21], who proposed a structural model for *disordered* metazeunerite.

Table 3. Unit-cell parameters refined from Single-Crystal X-ray Diffraction (SXRD) for zeunerite and metazeunerite.

Sample	S.G.	*a* (Å)	*c* (Å)	*V* (Å^3)	Locality	Ref.
Zeunerite						
VC2135	*P*4/*nnc*	7.183(1)	20.872(1)	1076.9(1)	Rabejac, Fr	-
VC2165	*P*4/*nnc*	7.177(1)	20.839(1)	1073.4(1)	Rabejac, Fr	-
VC2159	*P*4/*nnc*	7.145(1)	20.887(1)	1066.2(1)	Rabejac, Fr	-
U019	*P*4/*nnc*	7.173(1)	20.850(1)	1072.9(1)	Rabejac, Fr	-
U030	*P*4/*nnc*	7.123(1)	20.842(1)	1057.5(1)	Rabejac, Fr	-
U040	*P*4/*nnc*	7.151(1)	20.848(1)	1066.8(1)	Rabejac, Fr	-
-	*P*4/*nnc*	7.179(1)	20.857(1)	1075.1(1)	Synthetic	[20]
-	*I*4/*mmm*	7.175(1)	20.873(1)	1074.6(1)	Synthetic	[21]
Metazeunerite						
VC2139	*P*4/*n*	7.108(1)	8.729(1)	441.1(1)	Rabejac, Fr	-
VC2164	*P*4/*n*	7.101(1)	8.717(2)	439.5(1)	Rabejac, Fr	-
U029	*P*4/*n*	7.078(1)	8.701(1)	435.9(1)	Rabejac, Fr	-
U009	*P*4/*n*	7.087(1)	8.727(1)	438.3(1)	Rabejac, Fr	-
U040	*P*4/*n*	7.048(1)	8.696(1)	432.0(1)	Rabejac, Fr	-
U008	*P*4/*n*	7.111(1)	8.711(1)	440.5(1)	Rabejac, Fr	-
-	*P*4/*nmm*	7.106(10)	8.709(1)	439.8(1)	Synthetic †	[21]
-	$P4_2/nmc$	7.100	17.700	892.3	Rotava, Cz	[22]
-	*P*4/*n*	7.12	17.45	884.6	Majuba Hill, USA	[23]
-	?	7.104	17.45	880.6	Schwarzwald, De	[24]
-	?	7.080(2)	17.394(5)	871.9	Cínovec, Cz	[25]
-	?	7.113(1)	17.433(3)	882.0	Jáchymov, Cz	[26]
-	*P*4/*nnc*	7.106(1)	17.419(1)	879.7(1)	Synthetic ‡	[21]
-	*P*4/*n*	7.1094(1)	17.416(1)	880.3(1)	Synthetic	[20]

† *disordered* metazeunerite; ‡ *ordered* metazeunerite; S.G.: Space group; -: No catalogue number; ?: Space group not reported.

4.1.2. Nováčekite-I, Nováčekite-II and Metanováčekite—$Mg[(UO_2)(AsO_4)]_2(H_2O)_{12\text{-}8}$

Crystals of nováčekite-I/II and metanováčekite are usually semi-transparent; their colour is straw-yellow to green-yellow and sometimes brown-yellow. These minerals form tetragonal crystals tabular on {001}, up to 1 cm in length. A perfect cleavage on {001} exists. At first sight, these minerals are difficult to distinguish from their Ca analogue uranospinite. Nováčekite is often associated with zeunerite and uranospinite, and with U-free minerals, such as arsenolite, As_2O_3, and tyrolite, $Ca_2Cu_9(AsO_4)_4(CO_3)(OH)_8(H_2O)_{11}$.

Chemical compositions of nováčekite and metanováčekite are relatively constant, with few substitutions on the cationic *T* and *A* sites (Table 4). The *T* site is always practically fulfilled by As (1.97 to 1.98 *apfu*), without any significant amount of P or S and S (<0.02 *apfu*) (Figure 3). The *A* site is mainly occupied by Mg (0.85 to 0.94 *apfu*), which is partially replaced by a small amount of Cu (0.01 to 0.03 *apfu*). The content of Ca is very low but it remains constant (<0.02 *apfu*). Note that the cationic totals for the *A* site are below 1 for all samples (0.91 to 0.98 *apfu*); however, no other elements compatible with the autunite structure were detected. As there are few variations in composition between the different samples of nováčekite analyzed, the mean formula for all the samples is given by $(Mg_{0.91}Ca_{0.01}Ba_{0.01})_{\sum 0.93}[(U_{1.04}O_2)(As_{0.99}P_{0.01}O_4)]_2(H_2O)_{10}$.

Table 4. Chemical composition of nováčekite-II and metanováčekite.

Sample	Nováčekite-II				Metanováčekite
	U039	**VC2136**	**VC2151**	**VC2152**	**U015**
n	7	6	7	12	7
SO_3 wt %	0.02	0.04	0.00	0.04	0.08
SiO_2	0.01	0.04	0.00	0.03	0.00
As_2O_5	23.50	24.40	24.82	23.38	24.72
P_2O_5	0.16	0.13	0.14	0.11	0.06
Al_2O_3	0.01	0.01	0.03	0.01	0.00
CuO	0.22	0.17	0.08	0.06	0.05
FeO	0.04	0.02	0.02	0.07	0.07
MgO	3.55	4.06	4.13	3.78	4.01
CaO	0.06	0.05	0.06	0.10	0.07
BaO	0.11	0.09	0.05	0.06	0.03
Na_2O	0.03	0.01	0.03	0.05	0.00
UO_3	63.25	64.21	64.08	60.53	63.66
H_2O	9.33	9.70	9.82	9.28	7.82
Total	100.29	102.93	103.26	97.50	100.57
Cation numbers based on As + P + Si + S = 2 *apfu*					
S^{6+}	0.002	0.005	0.000	0.005	0.009
Si	0.002	0.006	0.000	0.005	0.000
As	1.974	1.972	1.982	1.975	1.983
P	0.022	0.017	0.018	0.015	0.008
Σ*T* site	2.000	2.000	2.000	2.000	2.000
Al	0.002	0.002	0.005	0.002	0.000
Cu	0.027	0.020	0.009	0.007	0.006
Fe^{2+}	0.005	0.003	0.003	0.009	0.009
Mg	0.850	0.936	0.940	0.910	0.917
Ca	0.010	0.008	0.010	0.017	0.012
Ba	0.007	0.005	0.003	0.004	0.002
Na	0.009	0.003	0.009	0.016	0.000
Σ*A* site	0.910	0.977	0.979	0.965	0.946
U^{6+}	2.135	2.085	2.056	2.055	2.052
H_2O	10	10	10	10	8

Refined unit-cell parameters for nováčekite and metanováčekite, as obtained from PXRD and SXRD, are provided in Table 5. These data are interesting as they indicate the presence of at least three types of nováčekite with different hydration state. From the most to the less hydrated species there are: nováčekite-I, $Mg[(UO_2)(AsO_4)]_2(H_2O)_{12}$; nováčekite-II, $Mg[(UO_2)(AsO_4)]_2(H_2O)_{10}$; and, metanováčekite, $Mg[(UO_2)(AsO_4)]_2(H_2O)_8$. These species can be differentiated on the basis of their main diffraction peak at 11.04, 10.03 and 8.89 Å for nováčekite-I, nováčekite-II and metanováčekite, respectively. The X-ray diffraction study indicates that the sample U039 contains a mixture of nováčekite-I and nováčekite-II. Unfortunately, no nováčekite I and metanováčekite single-crystals suitable for X-ray crystallographic studies were found. In the case of nováčekite-II, the most common observed species, *a* and *c* unit-cell parameters, are quite consistent for all the samples. However, the *b* unit-cell parameter, which is parallel to the stacking direction of the uranyl arsenate sheets, differs somewhat between the analyzed samples. The value of $b \approx 19.97$ Å (samples VC2151 and U039) is very close to the value reported for saléeite, the phosphate analogue of nováčekite-II. However, the value of $b \approx 20.45$ Å (samples VC2136 and VC2152) is not expected, as it does not correspond to the classical value reported for the nováčekite-saléeite series. The refined unit-cell parameters for nováčekite-I are in agreement with those reported for its synthetic analogue [27], and the refined unit-cell parameters for metanováčekite are in agreement with those that were reported for metanováčekite from Jáchymov [28], metarauchite, $Ni[(UO_2)(AsO_4)]_2(H_2O)_8$ [29], metakirchheimerite, $Co[(UO_2)(AsO_4)]_2(H_2O)_8$ [30], and metalodèvite, $Zn[(UO_2)(AsO_4)]_2(H_2O)_8$ [31].

Table 5. Refined unit-cell parameters of nováčekite-II, nováčekite-I and metanováčekite.

Sample	*a* (Å)/α (°)	*b* (Å)/β (°)	*c* (Å)/γ (°)	*V* (Å^3)	S.G.	Locality, Ref.
Nováčekite-I (12 H_2O)						
U039 †	7.276(6)/81.03(7)	7.213(6)/81.93(5)	11.226(6)/87.1(1)	576.0(5)	*P*-1	Rabejac, Fr
-	7.159(1)/81.39(1)	7.161(1)/81.18(1)	11.314(1)/88.9(1)	566.7(1)	*P*-1	Synthetic [27]
Nováčekite-II (10 H_2O)						
VC2136 *	7.142(1)	20.462(2)/89.92(1)	7.143(1)	1043.9(1)	$P2_1/n$	Rabejac, Fr
VC2151 *	7.138(1)	19.974(1)/90.44(1)	7.164(1)	1021.5(3)	$P2_1/n$	Rabejac, Fr
VC2152 *	7.157(1)	20.440(1)/90.02(1)	7.159(1)	1047.3(1)	$P2_1/n$	Rabejac, Fr
U039 †	7.121(5)	19.979(20)/91.08(9)	7.199(8)	1024(1)	$P2_1/n$	Rabejac, Fr
-	7.133(1)	20.085(3)/90.58(1)	7.157(1)	1025.3(3)	$P2_1/n$	Synthetic [27]
Metanováčekite (8 H_2O)						
U015 †	7.181(4)/72.96(4)	9.947(5)/85.74(3)	13.149(3)/83.1(1)	891.0(7)	*P*-1	Rabejac, Fr
-	7.201(5)/75.54(5)	9.755(5)/83.84(6)	13.27(6)/81.87(6)	891(1)	*P*-1	Jáchymov, Cz [28]

Unit-cell parameters refined from SXRD (*) and PXRD (†).

4.1.3. Uranospinite/Metauranospinite—$Ca[(UO_2)(AsO_4)]_2(H_2O)_{11\text{-}8}$

In the Rabejac deposit uranospinite occurs as transparent deep-yellow tabular crystals, while tabular crystals of metauranospinite are not translucent and exhibit a darker color. In uranospinite crystals, perfect and distinct cleavages occur on (001) and (100), respectively. Only the perfect cleavage on (001) is visible in the case of metauranospinite. The size of the crystals is usually 0.2–0.3 mm for both species. These minerals are observed in association with Cu- and Mg-bearing uranyl arsenates of the (meta-)autunite group, and with other uranyl minerals, such as umohoite and uranophane-α.

EPMA performed on uranospinite and metauranospinite samples show wide variations in composition, on both the *T* and *A* sites (Table 6). The occupancy of the *T* site by the $(AsO_4)^{3-}$ anionic group between 1.98 and 1.22 *apfu*, while the proportion of the $(PO_4)^{3-}$ anionic group varies between 0.01 and 0.76 *apfu*. The replacement of As by P indicates a solid solution extended towards autunite and meta-autunite. Replacement of As by Si or S is nearly nonexistent (<0.02 *apfu*) (Table 6, Figure 3). The *A* site is predominantly occupied by Ca (0.70 to 0.83 *apfu*), which is mainly accompanied by Mg (0.16 to 0.25 *apfu*) (Figure 4). Replacement of Ca by Mg is an indication of the occurrence of a solid-solution between uranospinite and nováčekite. However, as shown previously, the nováčekite samples from Rabejac are usually Ca-free (Table 4 and Figure 4).

Table 6. Chemical composition of uranospinite.

Sample	U033	U011	VC2140	VC2165	U008	VC2136	VC2152
n	12	10	4	7	7	9	22
SO_3 wt %	0.03	0.04	0.05	0.02	0.01	0.09	0.03
SiO_2	0.03	0.07	0.10	0.05	0.08	0.01	0.07
As_2O_5	24.79	22.47	14.86	24.35	23.10	24.04	23.88
P_2O_5	0.13	1.46	5.71	0.18	0.81	0.58	0.10
Al_2O_3	0.02	0.01	0.03	0.00	0.03	0.02	0.01
CuO	0.05	0.12	0.11	0.08	0.13	0.01	0.03
FeO	0.02	0.04	0.07	0.02	0.05	0.13	0.04
MgO	1.06	0.78	0.96	0.90	0.84	0.70	0.97
CaO	4.70	4.38	4.16	4.73	4.20	5.06	4.43
BaO	0.04	0.04	0.24	0.08	0.07	0.05	0.06
Na_2O	0.02	0.08	0.04	0.07	0.06	0.04	0.11
UO_3	62.94	64.34	59.38	62.29	63.46	62.48	62.15
H_2O	10.82	10.79	10.51	10.68	10.58	10.83	10.44
Total	104.65	104.62	96.22	103.45	103.42	104.04	102.32
Cation numbers based on As + P + Si + S = 2 *apfu*							
S^{6+}	0.003	0.005	0.006	0.002	0.001	0.010	0.004
Si	0.005	0.011	0.016	0.008	0.012	0.002	0.011
As	1.975	1.796	1.220	1.966	1.880	1.913	1.972
P	0.017	0.189	0.759	0.024	0.107	0.075	0.013
Σ*T* site	2.000	2.000	2.000	2.000	2.000	2.000	2.000
Al	0.004	0.002	0.006	0.000	0.006	0.004	0.002
Cu	0.006	0.014	0.013	0.009	0.015	0.001	0.004
Fe^{2+}	0.003	0.005	0.009	0.003	0.007	0.017	0.005
Mg	0.241	0.178	0.225	0.207	0.195	0.159	0.228
Ca	0.767	0.717	0.700	0.783	0.700	0.825	0.750
Ba	0.002	0.002	0.015	0.005	0.004	0.003	0.004
Na	0.006	0.024	0.012	0.021	0.018	0.012	0.034
Σ*A* site	1.029	0.942	0.979	1.028	0.945	1.021	1.027
U^{6+}	2.015	2.066	1.958	2.021	2.075	1.998	2.062
H_2O	11	11	11	11	11	11	11

As for autunite and meta-autunite, the water contents of uranospinite and metauranospinite are not well defined, as uranospinite easily and readily de-hydrate into metauranospinite in dry environment. Locock and Burns (2003) [32] report 11 water molecules *pfu* in hydrated autunite, and 7 water molecules *pfu* are reported in meta-autunite coming from the dehydration of synthetic autunite [33]. However, refinement of the crystal structure of natural meta-autunite, which should be considered as the phosphate analogue of metauranospinite indicates the presence of six water molecules [34]. It is likely that the dehydration of autunite yields to several *meta-autunite* species with different hydration states. Furthermore, the dehydration process is partially reversible, it is uncertain if all the lost water molecules would be recovered in the structure. In the present case, the interpretation of the chemical analyses was based on 11 water molecules *pfu*. The chemical formula of the P-free uranospinite from Rabejac is given by $(Ca_{0.75}Mg_{0.25})[(U_{1.01}O_2)(As_{0.99}P_{0.01}O_4)]_2(H_2O)_{11}$ (it is also the sample with the highest Mg amount), while the chemical formula of the P-rich uranospinite is $(Ca_{0.70}Mg_{0.22}Cu_{0.01}Fe_{0.01}Ba_{0.01}Na_{0.01})_{\sum 0.96}[(U_{0.98}O_2)(As_{0.61}P_{0.38}Si_{0.01}O_4)]_2(H_2O)_{11}$.

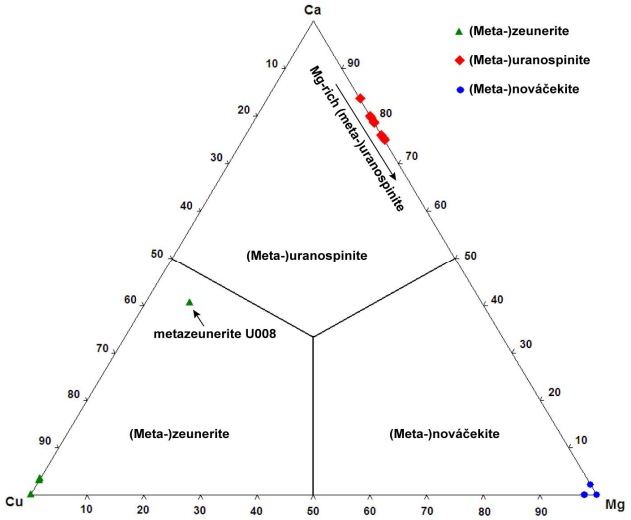

Figure 4. Ternary plot of the *A*-site occupancy of the members for the (meta-)autunite group from Rabejac.

Unfortunately it was not possible to find any single crystals that are suitable to perform crystallographic analyses on uranospinite and metauranospinite. Even single crystals with excellent optical properties, completely transparent (and thus supposed to be *fully* hydrated), and for which optical examinations under the polarizing microscope indicate that the mineral has biaxial optical anomalies (typical for autunite-type minerals), appear to be amorphous under the X-ray beam. As explained above, the water content of uranospinite and metauranospinite is not constant, and it may be assumed that several dehydration-hydration processes have altered the structure of the crystals, especially the organisation of the Ca atoms and of the water molecules occurring in the interlayer space.

The refinement of the unit-cell parameters from PXRD was also very difficult, and the uranospinite samples gave powder patterns with only a few analogies with those reported in the literature for synthetic uranospinite [35] and for meta-autunite [28,33,36–38]. Actually, the most intense peak (10.233 Å) that was observed is close to the most intense peak of synthetic hydrated autunite (10.356 Å [32]), than to that of meta-autunite (8.30–8.50 Å). Despite this similarity, the powder patterns obtained for uranospinite from Rabejac are not in agreement with that of autunite (even if one considers the P-As substitution), and therefore the refinement of the unit-cell parameters in the *Pnma* space group reported for autunite [32] gives only poorly accurate values: a = 14.11(4), b = 20.69(9), c = 6.87(1) Å, and V = 2007(17) Å^3. The obtained powder patterns suggest that all of the samples are actually constituted by a mixture of hydrated and dehydrated uranospinite crystals.

4.1.4. Heinrichite—$Ba[(UO_2)(AsO_4)]_2(H_2O)_{10}$

Heinrichite was only observed in sample U015, in which the heinrichite crystals form intimate intergrowths with crystal of nováčekite. Both minerals occur as light-yellow platy crystals flattened on {001}, which are up to 0.3 mm in length. In addition to the basal cleavage on (001), there is one distinct cleavage on (100). Actually, the identification of heinrichite was only made through EPMA, as the entirety of crystals that was observed on the rock sample was previously identified as nováčekite.

The chemical formula of the analyzed heinrichite sample is very close to the ideal formula reported for this mineral, $(Ba_{1.07}Al_{0.02}Na_{0.02}Ca_{0.01}Cu_{0.01})_{\sum 1.13}[(U_{1.10}O_2)(As_{0.99}P_{0.01}O_4)]_2(H_2O)_{10}$ (Table 7). Substitution of Ba by any other cation is not expected, as the autunite-type compounds that contain Ba differ from other autunite-type compounds that contain large cations [39]. The substitution of As by P is insignificant; however, it is inferred that heinrichite is isostructural with uranocircite [40].

As heinrichite crystals are intimately associated with nováčekite crystals it was not possible to isolate pure heinrichite material to perform PXRD, and all the analyzed single crystals have shown unit-cell parameters similar to those of the members of the saléeite-nováčekite series.

Table 7. Chemical composition of metauranocircite-I and heinrichite.

Sample	Metauranociricite-I	Heinrichite
	U012	**U015**
n	13	4
SO_3 wt %	0.03	0.01
SiO_2	0.00	0.00
As_2O_5	0.39	21.23
P_2O_5	15.16	0.09
Al_2O_3	0.14	0.09
CuO	0.09	0.08
FeO	0.10	0.04
MgO	0.03	0.00
CaO	0.03	0.05
BaO	15.71	15.35
Na_2O	0.06	0.05
K_2O	0.46	-
UO_3	61.94	58.94
H_2O	6.85	8.43
Total	100.99	104.36
Cation numbers based on As + P + Si + S = 2 *apfu*		
S^{6+}	0.003	0.001
Si	0.000	0.000
As	0.032	1.986
P	1.965	0.013
Σ*T* site	2.000	2.000
Al	0.025	0.018
Cu	0.010	0.010
Fe^{2+}	0.006	0.006
Mg	0.008	0.001
Ca	0.005	0.010
Ba	0.943	1.070
Na	0.018	0.016
K	0.091	-
Σ*A* site	1.106	1.131
U^{6+}	1.993	2.203
H_2O	7	10

4.1.5. Metauranocircite-I—$Ba[(UO_2)(PO_4)]_2(H_2O)_7$

One sample (U012) of metauranocircite-I has been studied. The crystals of metauranocircite-I occur as green-yellow to brown-yellow thick tabular crystals, with a typical pearly or waxy lustre. Two cleavage planes on (001) and (010) are observed. The crystals are particularly large; some of them reach more than 1 cm in length.

EPMA show that the chemical composition of metauranocircite-I is very close to the ideal formula reported for this mineral, $(Ba_{0.94}K_{0.09}Al_{0.02}Na_{0.02})_{\sum 1.07}[(U_{0.99}O_2)(P_{0.98}As_{0.02}O_4)]_2(H_2O)_7$ (Table 7), with none significant cationic replacement.

The unit-cell parameters for metauranocircite-I from Rabejac was refined from SXRD diffraction (Table 8). The unit-cell parameters are in good agreement with those that were previously reported for natural metauranocircite-I [41] and for the synthetic analogues of metauranocircite-I [40]. Unfortunately, it was impossible to refined a good structural model due to the high disorder of the Ba cations and H_2O groups located in the interlayer space of the structure.

Table 8. Refined unit-cell parameters of metauranocircite-I.

Sample	*a* (Å)	*b* (Å)	*c* (Å)	β (°)	*V* (Å^3)	S.G.	Locality, Ref.
U012	6.951(1)	17.605(1)	6.961(1)	90.11(1)	851.7(1)	$P2_1$	Rabejac, Fr [42]
-	6.965(3)	17.65(1)	6.964(2)	90.00	856.1(3)	$P2_1$	Bota-Burum, Kz [41]
-	6.942(3)	17.634(6)	6.952(2)	90.02(1)	851.2(5)	$P2_1$	Synthetic [40]

4.1.6. Arsenuranospathite—$Al[(UO_2)(AsO_4)]_2F(H_2O)_{20}$

Arsenuranospathite forms light-green to yellow-greenish transparent bladed crystals showing the {100}, {010}, and {001} forms. The crystals can reach up to 0.5 mm in length. A perfect (001) cleavage plane is observed, as well as two other weaker cleavage planes parallel to (100) and (010). Emerald-green platy crystals of zeunerite are associated with arsenuranospathite; these two minerals form intimate intergrowths, which probably mean that both of the species have crystallized simultaneously. An undetermined powdery yellowish mineral is also occurring in close association with arsenuranospathite and zeunerite. Energy-dispersive X-ray spectrometric analysis shows that this compound contains high amounts of U, S, and Ca, as well as a low amount of Fe; it may correspond to rabejacite. Several crystals of arsenuranospathite are completely coated by these yellowish crystals, indicating that this mineral crystallized during a later stage [42].

Chemical analyses point out that a part of As is replaced by P, thus confirming the common substitution between these cations in tetrahedral coordination, and the solid solution between arsenuranospathite and uranospathite (Table 9) [42,43]. The F content reaches 0.77 *apfu*, the U content is close to 2 *apfu*, and the Al content is close to 1 *apfu*. The other cations (Fe, Mg, Ca, Ba, and Na) occur in very low amounts, and do not play a significant crystal-chemical role in the structure. Nevertheless, according to the light greenish color of the crystals of arsenuranospathite and the Cu-bearing mineral (zeunerite) associated with arsenuranospathite, it may be possible that a small amount of Cu occurs in the interlayer space of arsenuranospathite. The empirical formula of the studied sample is $(Al_{1.02}Cu_{0.01})[(U_{0.98}O_2)(As_{0.89}P_{0.08}Si_{0.02}S_{0.01})O_4]_2(F_{0.77}OH_{0.05})(H_2O)_{20.18}$. These data are in agreement with those reported recently [44,45].

Unit-cell parameters for arsenuranospathite refined from SXRD in the non-centrosymmetric space group *Pnn*2 are: a = 29.926(1), b = 7.1323(1), c = 7.1864(1) Å, and V = 1533.91(6) $Å^3$ (Table 10). These unit-cell parameters are in good agreement with those that were previously reported for arsenuranospathite [45,46] and for uranospathite [43,46]. The crystal structure was solved for the first time, thus confirming the presence of 20 water molecules *pfu*, and the isomorphism with uranospathite [42].

Table 9. Chemical composition of arsenuranospathite.

Sample	VC2135
n	20
SO_3 wt %	0.08
SiO_2	0.22
As_2O_5	21.30
P_2O_5	1.27
Al_2O_3	5.44
CuO	0.11
FeO	0.02
MgO	0.01
CaO	0.05
BaO	0.02
Na_2O	0.05
UO_3	58.82
F	1.52
H_2O *	19.30
O=F	−0.64
Total	107.57
Cation numbers based on As + P + Si + S = 2 *apfu*	
S	0.013
Si	0.036
As	1.779
P	0.172
Σ*T* site	2.000
Al	1.024
Cu	0.013
Fe^{2+}	0.003
Mg	0.002
Ca	0.008
Ba	0.001
Na	0.015
Σ*A* site	1.111
U^{6+}	1.975
F	0.768

* H_2O content was calculated on the basis of (H_2O + F + OH) = 21 (from [42]).

Table 10. Comparison of the crystallographic parameters of arsenuranospathite and uranospathite.

a (Å)	*b* (Å)	*c* (Å)	*V* (Å^3)	S.G.	Locality	Ref.
Arsenuranospathite						
29.926	7.132	7.186	1533.9	*Pnn*2	Rabejac, Fr	[42]
30.070	7.147	7.193	1545.8	*Pnn*2	Menzenschwand, De	[45]
7.16	7.16	30.37	1556.9	$P4_2/n$	Menzenschwand, De	[46]
Uranospathite						
30.020	7.008	7.049	1483.1	*Pnn*2	Vénachat, Fr	[43]
7.00	7.00	30.02	1471.0	$P4_2/n$	Cornwall, UK	[46]

4.2. Uranyl Molybdates

Umohoite, $[(UO_2)(MoO_4)(H_2O)](H_2O)$, occurs in two distinct habitus. In the first one, umohoite forms bright red nodules up to 0.1 mm, which are actually constituted by a myriad of sub-micrometric platy crystals. The second habitus is characterized by greenish-black to black platy crystals with metallic luster. The red nodules are observed in association with calcurmolite, while the black plates are accompanied with yellow plates of uranospinite, and with tiny brown-green crystals of an unidentified Cu–U–Mo phase (probably deloryite). Calcurmolite, $Ca_2(UO_2)_3(MoO_4)_2(OH)_6(H_2O)_n$,

forms millimetric bright yellow nodules, which are constituted by a radial aggregation of tiny prismatic crystals with a section of 1–5 μm.

The chemical composition of umohoite and calcurmolite from Rabejac are given in Table 11. The empirical formulae of umohoite and calcurmolite were calculated on the basis of (Mo + S) = 1 and 2 *apfu*, respectively. Even if the chemical formula of umohoite contains only the cations U and Mo, some umohoite samples are reported with significant amounts of Ca (2.51 wt % CaO [47]), and traces of Ni and Mg [48]. These impurities seem to be responsible for the colour variations that were observed for umohoite crystals. In the present study, appreciable amounts of Cu (2.68 wt % CuO), Ca (0.47 wt % CaO), P (0.35 wt % P_2O_5), and Si (0.18 wt % SiO_2), are detected. The Mg content is very low (0.10 wt % MgO), and Ni was not detected at all. The impurity in Cu may be attributed to a contamination from deloryite, $Cu_4(UO_2)Mo_2O_8(OH)_6$, while the impurity in Ca may come from the presence of uranospinite. However, the uranyl molybdate sheets observed in the structure of umohoite are based upon the uranophane anion-topology [49]. This anion topology is very versatile and it accepts a lot of different cations (e.g., Si, P, Ca, Te). Moreover, the umohoite structure contains two symmetrically distinct interlayers that could be responsible for the accommodation of cations other than U or Mo.

Table 11. Chemical composition of umohoite and calcurmolite.

Sample	Umohoite	Calcurmolite
	VC2160	VC2161
n	6	11
MoO_3 wt %	30.93	22.44
SO_3	0.06	0.01
SiO_2	0.18	0.02
As_2O_5	0.01	0.04
P_2O_5	0.35	0.10
Al_2O_3	0.07	0.01
CuO	2.68	0.15
FeO	0.08	0.05
MgO	0.10	0.03
CaO	0.47	3.49
BaO	0.10	0.09
Na_2O	0.01	0.04
UO_3	60.82	69.11
H_2O	3.91	11.25
Total	99.78	106.83
Mo^{6+}	0.991	1.998
S^{6+}	0.009	0.002
Σ*M* site*	1.000	2.000
Si	0.027	0.008
As^{5+}	0.000	0.004
P	0.023	0.018
Al	0.007	0.002
Cu	0.155	0.023
Fe^{2+}	0.005	0.008
Mg	0.011	0.009
Ca	0.039	0.799
Ba	0.003	0.008
Na	0.002	0.016
U^{6+}	0.981	3.100
H_2O	2	8

* Cation numbers based on Mo + S = 1 and 2 *apfu* for umohoite and calcurmolite, respectively.

Calcurmolite is a poorly characterized mineral and its correct chemical formula remains uncertain. Deliens (1992) [50] provided chemical and crystallographic studies of calcurmolite from Rabejac. Comparison between these data and the data collected on calcurmolite samples from the former USSR [51,52], indicates many discrepancies in the X-ray powder diffraction patterns, as well as in the chemical composition (U:Mo ratio) of the different samples. It was presumed that calcurmolite described from materials coming from former USSR and Rabejac are actually different species [50].

For the calcurmolite from Rabejac, Deliens (1992) [50] reports the chemical formula $Ca(UO_2)_4(MoO_4)_3(OH)_4(H_2O)_8$, with 65.48 wt % UO_3, 21.62 wt % MoO_3, and 3.20 wt % CaO. Recently, on the basis of electron-microprobe analyses of samples from Kazakhstan and Armenia, Sidorenko et al. (2005) [53] provide a revised formula for calcurmolite, $(Ca,Na)_2(UO_2)_3(MoO_4)_2(OH)_6(H_2O)_n$, with 62.85 wt % UO_3, 20.80 wt % MoO_3, 5.7 wt % CaO, and 0.72 wt % Na_2O (Table 12). X-ray powder diffraction patterns of calcurmolite from Rabejac [50] and from Kazakhstan and Armenia [53] show a lot of similarities, but cannot be considered as being identical. In the present work, the formula of calcurmolite is reported as $(Ca_{0.80}Na_{0.02}Cu_{0.02})_{\sum 0.84}(U_{1.03}O_2)_3(Mo_{1.00}O_4)_2(OH)_{4.20}(H_2O)_8$, with 69.11 wt % UO_3, 22.44 wt % MoO_3, and 3.49 wt % CaO (Table 12). This formula (U:Mo = 3:2, Ca close to 1 *apfu*) is different from that reported by Sidorenko et al. (2005) (U:Mo = 3:2, Ca = 2 *apfu*) [53], but is very close to that reported by Deliens (1992) (U:Mo = 4.2:2.7 ≈ 3:2, Ca = 1 *apfu*) [50].

Table 12. Comparison of the chemical data reported for calcurmolite.

Formula	wt % CaO	wt % UO_3	wt % MoO_3	Ca:U:Mo	Ref.
$(Ca,Na)_2(UO_2)_3(MoO_4)_2(OH)_6(H_2O)_n$	5.70	62.85	20.80	2:3:2	[53]
$Ca(UO_2)_4(MoO_4)_3(OH)_4(H_2O)_8$	3.20	65.48	21.62	1:4:3	[50]
$Ca(UO_2)_3(MoO_4)_2(OH)_4(H_2O)_8$	3.49	69.11	22.44	1:3:2	-

Unit-cell parameters that were refined from powder X-ray diffraction of umohoite and calcurmolite are listed in Table 13. In the case of umohoite, the larger difference is observed for the *c* crystallographic parameters, in comparison with the data provided by Krivovichev and Burns (2000) [49]. As shown in the structural model, the *c* crystallographic parameter is perpendicular of the stacking of uranyl-molybdate sheets, and therefore this parameter is very sensitive to the cationic and water content of the interlayer space. As explained above, umohoite from Rabejac contains a lot of impurities (Mg, Ca, P, Si), which affect the structure and add some cationic disorder in the interlayer space. It results that single crystals analyzed are poorly crystallized, giving only a few diffraction peaks and a larger *c* parameter.

Table 13. Refined unit-cell parameters of umohoite and calcurmolite.

	Umohoite		Calcurmolite		
	This study *	[49] *	This study †	[53] †	[53] †
a (Å)	6.34(4)	6.3748(4)	16.76(1)	16.30(3)	16.31(3)
b (Å)	7.55(3)	7.8287(5)	24.822(7)	25.490(5)	25.50(6)
c (Å)	14.14(8)	14.628(1)	20.08(1)	19.506(6)	19.50(6)
α (°)	88.9(4)	82.64(1)	90.00	90.00	90.00
β (°)	83.1(5)	85.95(1)	90.01(8)	90.17	90
γ (°)	89.8(4)	89.91(1)	90.00	90.00	90.00
V (Å^3)	672(6)	694.52(8)	8357(10)	8104	8110
S.G.	*P*-1	*P*-1	*P*2/*m*	*P*2/*m*	*P*2/*m*
Locality	Rabejac, Fr	Former USSR	Rabejac, Fr	Kyzyl-Sai, Kz	Kadjaran, Am

Unit-cell parameters refined from SCXD (*) and PXRD (†).

The data obtained on calcurmolite are interesting, as the *b* and *c* crystallographic parameters differ from the values that were reported by Sidorenko et al. (2005) [53]. This observation confirms the assumption of Deliens (1992) [50] and the chemical data collected in the present study, showing that

calcurmolite samples from former USSR and Rabejac are actually related but are different mineral species (Table 13). Note that refinement of the unit-cell parameters in the orthorhombic space group *Pmmm* gives the same values for the *a*, *b*, and *c* parameters.

4.3. Uranyl-Oxide Hydroxy-Hydrates

Becquerelite and billietite are relatively common minerals in the sample from Rabejac. Crystals of becquerelite are transparent, canary-yellow to yellow-orange, and from prisms tabular on {001}, or thick laths. Crystals of billietite are also transparent and yellow-orange. They are tabular on {001} and show sometimes a pseudohexagonal shape. In general, both of the minerals are similar; however, the crystals of billietite are usually thicker. Both species form crystals up to about 1 mm long. Becquerelite is observed alone or in association with billietite, while billietite is often found in association with baryte, uranophane-α, and occasionally with uraninite.

The unit-cell parameters of both becquerelite and billietite are provided in Table 14, and they are in complete agreement with the data previously reported in the literature [54–57]. The refinements of the crystal structure of becquerelite and billietite from Rabejac are provided in the Supplementary Materials (Tables S1–S7, Figures S1–S4).

Table 14. Unit-cell parameters of becquerelite and billietite.

a (Å)	*b* (Å)	*c* (Å)	*V* (Å^3)	S.G.	Locality	Ref.
Becquerelite						
13.862	12.377	14.946	2564.3	$Pn2_1a$	Rabejac, Fr	This study
13.860	12.300	14.920	2543.5	$Pn2_1a$	Shinkolobwe, DRC	[55]
13.838	12.378	14.924	2556.3	$Pn2_1a$	Shaba, DRC	[56]
13.852	12.383	14.930	2563.1	$Pn2_1a$	Synthetic	[57]
Billietite						
12.083	30.189	7.151	2608.5	$Pbn2_1$	Rabejac, Fr	This study
12.072	30.167	7.145	2602.2	$Pbn2_1$	Shinkolobwe, DRC	[56]
12.094	30.211	7.156	2614.7	$Pbn2_1$	Shaba, DRC	[54]

4.4. Liebigite-$Ca_2[(UO_2)(CO_3)_3](H_2O)_{11}$

Observed in only one sample (U016), liebigite occurs as completely transparent, greenish-yellow to yellow, rounded blocky crystals, up to 0.5 mm. The crystals of liebigite are found to be in close association with colorless rhombohedra of calcite.

The unit-cell parameters refined from SXRD single-crystal X-ray diffraction are provided in Table 15. They are in agreement with the date reported by Mereiter (1982) [58] and Plášil et al. (2006) [59]. The refinement of the crystal structure of liebigite from Rabejac is provided in the Supplementary Materials (Tables S8–S13, Figures S5 and S6). This refinement indicates the presence of 11 water molecules per unit formula, and therefore confirms undoubtedly the assumption of Mereiter (1982) [58].

Table 15. Unit-cell parameters of liebigite.

a (Å)	*b* (Å)	*c* (Å)	*V* (Å^3)	S.G.	Locality	Ref.
17.573	16.737	13.718	4034.7	*Aba*2	Rabejac, Fr	This study
16.699	17.557	13.697	4015.7	*Bba*2	Jáchymov, Cz	[58]
16.682	17.590	13.652	4006.9	*Ama*2	Horní Slavkov, Cz	[59]

On the purpose to understand the crystallization process of uranyl carbonate minerals, it is interesting to compare the crystal structure of liebigite [58] to that of fontanite, which is the other Ca-bearing uranyl carbonate that was observed in Rabejac (the crystal structure of urancalcarite is still unknown). The structure of liebigite and fontanite are fundamentally different, the first one contains uranyl tricarbonate clusters, while the second one is based on uranyl carbonate sheets showing the phosphuranylite anion topology [3]. In addition, the connectivity of the Ca polyhedra relatively to

the uranyl carbonate units is different. In liebigite the Ca polyhedra are sharing edges with the UrO_6 and CO_3 polyhedra, while in the fontanite the Ca polyhedra are located between the uranyl carbonate sheets and are sharing corners with the uranyl ions from two adjacent sheets. These divergences are explained by the special conditions (relatively more acidic) required for the crystallization of fontanite and minerals based on uranyl-carbonate sheets [3].

5. Evolution of the Supergene Mineralization in the Rabejac Deposit

The origin of the uranium in the Lodève basin is still debatable and several hypotheses are discussed in the literature. The first hypothesis is a syngenetic process that is related to the erosion of the uranium-bearing granitic plutons of the Central Massif [60,61]. The second hypothesis is an origin from deep layers that have been affected by hydrothermal activities. The hydrothermal alteration has occurred through the major faults of the basement and before the beginning of the Permian sedimentation (~299 Ma) [62]. The third hypothesis is based on acid volcanism (ignimbrite), which is often linked with a uranium supply. This hypothesis is corroborated by the presence of volcanic ash layers and the abundance of molybdenum and zirconium in the Thuringian series (~270 Ma) [12,63].

Despite the fact that the origin of the uranium is not clear, the emplacement of the uranium deposits is correlated with the migration of the bitumen coming from the maturation of the organic matter trapped by the Permian sediments [12]. Uranium was concentrated during the Autunian-Saxonian sedimentation (~299 Ma), and the diagenesis occurring during the Thuringian (more than 2000 m of sediments) leads to the migration of bitumen and uranium along the faults network oriented east-west. U–Pb geochronological studies indicated two phases of uranium remobilization afterwards. The first uranium migration has occurred around 173 Ma (Lias) and the second around 110 Ma (Aptian-Albian boundary) [64].

The mineral associations that were observed in the Rabejac mine are typical of the supergene alteration zone of the uranium deposits. These secondary uranyl minerals show a wide diversity, especially in the fault zones where the oxido-reduction processes have occurred deeply, and therefore, all the succession in the alteration products of the uraninite is observed [8]. Firstly, in close association with uraninite (variety pitchblende), schoepite, vandendriesscheite, fourmarierite, masuyite, becquerelite and billietite are observed. These uranyl-oxide-hydroxy-hydrate minerals are very typical products of initial in-situ alteration of uraninite [65–67]. The presence of Pb-uranyl-oxide minerals (vandendriesscheite, fourmarierite, and masuyite) indicates that the uraninite is an *old uraninite*, as the majority of Pb is radiogenic, coming from the decay of uranium [66,68]. The small red plates of masuyite are often associated with uranyl-silicate sklodowskite [8]. The occurrence of the rare billietite is an evidence that the Ba activity was greater than the Ca activity during some period of the weathering.

Following the crystallization of uranyl-oxide-hydroxy-hydrate minerals, the formation of uranyl silicate phases is a common step as the Si^{4+} activity is increasing due to the alteration of the silicate minerals from the surrounding rocks [69]. In the Rabejac deposits, the uranyl silicates are characterized only by minerals of the uranophane group: uranophane-α, uranophane-β, kasolite, sklodowskite, and cuprosklodowskite. Some samples show an association between uranophane-α, rutherfordine, and zeunerite. Soddyite is not reported in the Rabejac deposit, and was not observed in the samples that are investigated in the present study.

The weathering processes affecting the uraninite have also lead to the formation of several uranyl carbonates. The most common phase is the metal-free carbonate rutherfordine, often found associated with uranophane-α. Crystallization of rutherfordine indicates an increase of the pCO_2 values and a near neutral to acid pH [66,70]. The increase of the pH (>8) leads to the formation of uranyl carbonates with UO_2:CO_3 ratio of 1:3, and especially of liebigite. The other observed uranyl carbonates are fontanite, which was discovered for the first time in the Rabejac deposit [2], and the very rare urancalcarite [71]. The UO_2:CO_3 ratio of these two species is uncommon, 3:2 and 3:1 for fontanite and urancalcarite, respectively. The conditions occurring at the moment of crystallization of

these phases are not clear; however, the crystallization of fontanite and urancalcarite can be considered as an indication of the increase of Ca activity, a pH below 6, and a slight decrease of the pCO_2 value, in comparison to the conditions leading to the formation of rutherfordine [66,70].

Despite the fact that uranyl phosphates constitute the most diverse group of uranyl minerals in the world, they are relatively scarce in the Rabejac deposit. Only autunite, saléeite, torbernite, and uranocircite-I are observed, as well as their dehydrated equivalent. Minerals of the phosphuranylite group, which are indicators of alkaline and neutral condition (pH > 7), are not reported [72]. The scarcity of phosphates of the autunite-group minerals is explained by the low P activity in the ground water due to the low amount of primary phosphate-bearing minerals (e.g., apatite) in the host rocks.

As shown in the mineralogical description part, the uranyl arsenates are very abundant in the Rabejac deposit and nearly all the uranyl arsenates of the autunite group can be observed. The origin of As is the sulphides and arsenides (such as chalcocite, bornite, domeykite, and koutekite) concentrated in the schists of the Thuringian series [11]. The high arsenic activity has also lead to the formation of secondary arsenolite in close association with uranyl arsenates, such as nováčekite and heinrichite. Uranyl arsenates are often found in association with uranyl phosphates, uranyl silicates, and uranyl sulphates, and some remarkable samples show close association between three different uranyl arsenates (e.g., zeunerite (Cu), uranospinite (Ca) and nováčekite (Mg)). The Rabejac deposit is also the type locality, as well as the Talmessi mine (Iran), of the mixed-valence uranyl arsenite-arsenate mineral seelite. This mineral does not belong to the autunite nor to the phosphuranylite group, as its structure is based upon sheets showing the uranophane-anion topology. The formation conditions of this mineral are unclear; in the Talmessi mine seelite occurs in association with arsenide (nickeline, NiAs) but also with arsenates (e.g., annabergite, $Ni_2(AsO_4)_2(H_2O)_8$) [4]. It can be assumed that local reducing conditions have allowed for the crystallization of seelite. Moreover, the uranophane-type sheets allow to stabilize the $(As^{3+}O_3)^{3-}$ anionic group, and to prevent its oxidation into the $(As^{5+}O_4)^{3-}$ anionic group, even under the oxidizing conditions of the surface.

Finally, the Rabejac deposit is characterized by the presence of uranyl vanadates (sengierite and tyuyamunite) and rare uranyl molybdates minerals (calcurmolite, iriginite, and umohoite). In the present study, tyuyamunite was observed in association with mottramite, $PbCu(VO_4)(OH)$. V is certainly coming from the alteration of the organic-rich shales located in the Autunian and Saxonian series [68], while Mo is likely coming from the alteration of molydenite (MoS_2) and Mo-rich sulphides concentrated in the schists of the Thuringian series.

Supplementary Materials: The following are available online at http://www.mdpi.com/2075-163X/8/9/414/s1. Figure S1: Representation of the sheet of uranyl polyhedra (α-U_3O_8) occurring in the structure of becquerelite. Yellow: UO_7 polyhedra, red: O^{2-} atoms, black: $(OH)^-$ groups. Figure S2: Structure of becquerelite projected along [100] and showing the connectivity between the sheets and the Caϕ_8 polyhedra. Yellow: UO_7 polyhedra, bleu: Caϕ_8 polyhedra, red: O^{2-} atoms and H_2O groups, black: $(OH)^-$ groups. Figure S3: The structural sheets of uranyl polyhedra occurring in the structure of billietite: (a) α-U_3O_8 and (b) β-U_3O_8-type sheet. Yellow: UO_7 polyhedra, orange: UO_6 polyhedra, red: O^{2-} atoms, black: $(OH)^-$ groups. Figure S4: Structure of billietite projected along [001] and showing the connectivity between the sheets and the Baϕ_{10} polyhedra. Yellow: Uϕ_7 polyhedra, orange: Uϕ_6 polyhedra, green: Baϕ_{10} polyhedra, red: O^{2-} atoms and H_2O groups, black: $(OH)^-$ groups. Figure S5: General view projected along the *c* axis of the structure of liebigite, showing the uranyl tricarbonate clusters connected together via the Ca polyhedra. Yellow: UO_8, green: CO_3, green: Ca atoms, red: O^{2-} atoms, white: H^+ atoms. Figure S6: Detailed view of the connectivity around the Ca polyhedra: (**a**) $Ca(1)O_4(H_2O)_4$, (**b**) $Ca(2)O_3(H_2O)_4$ and (**c**) $Ca(3)O_4(H_2O)_4$. Same legend as Figure S5. Table S1: Experimental details for the single-crystal X-ray diffraction study of becquerelite and billietite; Table S2: Atom fractional coordinates, isotropic and anisotropic atom displacement parameters ($Å^2$) for becquerelite. Table S3: Selected bond distances for becquerelite. Table S4: The bond-valence analysis (*vu*) for becquerelite. Table S5: Atom fractional coordinates, isotropic and anisotropic atom displacement parameters ($Å^2$) for billietite. Table S6: Selected bond distances for billietite. Table S7: The bond-valence analysis (*vu*) for billietite. Table S8: Experimental details for the single-crystal X-ray diffraction study of liebigite. Table S9: Atom coordinates and isotropic displacement parameters ($Å^2$) for liebigite. Table S10: Atom anisotropic displacement parameters ($Å^2$) for liebigite. Table S11: Selected bond

distances (Å) in the structure of liebigite. Table S12: Hydrogen-bond geometry in the structure of liebigite. Table S13: Bond-valence table (*vu*) for liebigite from Rabejac, France.

Author Contributions: F.D. performed all the experiments, analyzed the data and wrote the manuscript; F.H. and S.P. supported the project and contributed to manuscript writing.

Funding: This research was funded by a FRIA PhD grant number 93482 (FRS.-F.N.R.S., Belgium).

Acknowledgments: Many thanks to the National Museum of Natural History of Luxembourg for the loan of specimens. We also thank Jean-Luc Devidal of the Laboratoire Magmas et Volcans, Université Blaise Plascal, Clermont-Ferrand, France, for his assistance for the electron-microprobe analyses.

Conflicts of Interest: The authors declare no conflict of interest.

References

1. Olds, T.A.; Plášil, J.; Kampf, A.R.; Simonetti, A.; Sadergaski, L.R.; Chen, Y.S.; Burns, P.C. Ewingite: Earth's most complex mineral. *Geology* **2017**, *45*, 1007–1010. [CrossRef]
2. Deliens, M.; Piret, P. La fontanite, carbonate hydraté d'uranyle et de calcium, nouvelle espèce minérale de Rabejac, Hérault, France. *Eur. J. Mineral.* **1992**, *4*, 1271–1274. [CrossRef]
3. Hughes, K.A.; Burns, P.C. A new uranyl carbonate sheet in the crystal structure of fontanite, $Ca[(UO_2)_3(CO_3)_2O_2](H_2O)_6$. *Am. Mineral.* **2003**, *88*, 962–966. [CrossRef]
4. Bariand, P.; Bachet, B.; Brassy, C.; Medenback, O.; Deliens, P.; Piret, P. Seelite—A new uranium mineral from the Talmessi Mine, Iran, and Rabejac, France. *Mineral. Rec.* **1993**, *24*, 463–467.
5. Piret, P.; Piret-Meunier, J. Structure de la seelite de Rabejac (France). *Eur. J. Mineral.* **1994**, *6*, 673–677. [CrossRef]
6. Deliens, M.; Piret, P. La rabejacite, $Ca(UO_2)_4(SO_4)_2(OH)_6{\cdot}6H_2O$, nouveau sulfate d'uranyle et de calcium des gîtes du Lodévois, Hérault, France. *Eur. J. Mineral.* **1993**, *5*, 873–877. [CrossRef]
7. Plášil, J.; Dušek, M.; Čejka, J.; Sejkora, J. The crystal structure of rabejacite, the Ca^{2+}-dominant member of the zippeite group. *Mineral. Mag.* **2014**, *78*, 1249–1264. [CrossRef]
8. Lebrun, P.; Cesbron, F.; Le Cléac'h, J.M.; Lebocey, J. *Minéraux Uranifères. Uraninite et Minéraux Secondaires Dérivés ou Associés*; Minéraux & Fossiles Hors-Série; Mineraux et Fossiles: Orsival, France, 2009; p. 176. (In French)
9. Bavoux, B.; Guiollard, P.C. *L'uranium du Lodévois (Hérault)*; Bihet Press: Bizanos, France, 1999; p. 68. (In French)
10. Caubel, A. Minéralogie du gisement d'uranium de Rabejac, Hérault. *Le Règne Minéral* **1997**, *13*, 5–18. (In French)
11. Deliens, M.; Henriot, O.; Mathis, V.; Caubel, A. *Minéraux des Gisements D'uranium du Lodévois*; Association française de Microminéralogie: Paris, France, 1990; p. 60. (In French)
12. Mathis, V.; Robert, J.P.; Saint-Martin, J. Géologie et métallogénie des gisements d'uranium du bassin permien de Lodève (Sud du Massif Central français). *Chronic. Min. Res. Explor.* **1990**, *499*, 31–41. (In French)
13. Burnham, C.W. *LCLSQ Version 8.4, Least-Squares Refinement of Crystallographic Lattice Parameters*; Department of Earth & Planetary Sciences, Harvard University: Cambridge, MA, USA, 1991; p. 24.
14. Agilent Technologies. *CrysAlis CCD and CrysAlis RED*; Oxford Diffraction Ltd.: Yarnton, Oxfordshire, UK, 2012.
15. Sheldrick, G.M. Crystal structure refinement with SHELXL. *Acta Cryst.* **2015**, *71*, 3–8.
16. Wilson, A.J.C. (Ed.) *Ternational Tables for Crystallography. Volume C: Mathematical, Physical and Chemical Tables*; Kluwer Academic: Dordrecht, The Netherland, 1992.
17. Brown, I.D.; Altermatt, D. Bond-valence parameters obtained from a systematic analysis of the inorganic crystal structure database. *Acta Cryst.* **1985**, *41*, 244–247. [CrossRef]
18. Burns, P.C.; Ewing, R.C.; Hawthorne, F.C. The crystal chemistry of hexavalent uranium: Polyhedron geometries, bond-valence parameters, and polymerization of polyhedra. *Can. Mineral.* **1997**, *35*, 1551–1570.
19. Plášil, J.; Sejkora, J.; Čejka, J.; Škoda, R.; Goliáš, V. Supergene mineralization of the Medvědín uranium deposit, Krkonoše Mountains, Czech Republic. *J. Geosci.* **2009**, *54*, 15–56. (In French) [CrossRef]
20. Locock, A.J.; Burns, P.C. Crystal structures and synthesis of the copper-dominant members of the autunite and meta-autunite groups: Torbernite, zeunerite, metatorbernite and metazeunerite. *Can. Mineral.* **2003**, *41*, 489–502. [CrossRef]
21. Hennig, C.; Reck, R.; Reich, T.; Roßberg, A.; Krausi, W.; Sieler, J. EXAFS and XRD investigations of zeunerite and meta-zeunerite. *Z. Kristallogr.* **2003**, *218*, 37–45. [CrossRef]
22. Hanic, F. The crystal structure of meta-zeunerite $Cu(UO_2)_2(AsO4)_2{\cdot}8H_2O$. *Czech. J. Phys.* **1960**, *10*, 169–181. [CrossRef]

23. Ross, M.; Evans, H.T.; Appleman, D.E. Studies of torbernite minerals. II. Crystal structure of meta-torbernite. *Am. Mineral.* **1964**, *49*, 1603–1621.
24. Walenta, K. *Torbernit Aus der Grube Clara Bei Oberwolfach (Schwarzwald)*; Hermann Aldinger Festschrift: Stuttgart, Germany, 1962; pp. 185–190.
25. Jansa, J.; Novák, F.; Pauliš, P.; Scharmová, M. Supergene minerals of the Sn–W Cínovec deposit, Krušné hory Mts. (Czech Republic). *Bull. Mineral. Petrolog. Odd. Nár. Muz.* **1998**, *6*, 83–101.
26. Ondruš, P.; Veselovský, F.; Hloušek, J.; Skála, R.; Vavřín, I.; Frýda, J.; Čejka, J.; Gabašová, A. Secondary minerals of the Jáchymov (Joachimsthal) ore district. *J. Czech. Geol. Soc.* **1997**, *42*, 3–76. (In French)
27. Locock, A.; Burns, P.C.; Flynn, T.M. Divalent transition metals and magnesium in structures that contain the autunite-type sheet. *Can. Mineral.* **2004**, *42*, 1699–1718. [CrossRef]
28. Plášil, J. Crystal Chemistry of Selected Natural Hydrated Uranyl Arsenates and Phosphates of Divalent Transition Metals and Magnesium. Master's Thesis, Charles University, Prague, Czech Republic, June 2009.
29. Plášil, J.; Sejkora, J.; Cejka, J.; Novák, M.; Viñals, J.; Ondruš, P.; Veselovský, F.; Škácha, P.; Jehlicka, J.; Goliáš, V. Metarauchite, $Ni(UO_2)_2(AsO4)_2{\cdot}8H_2O$, from Jáchymov, Czech Republic, and Schneeberg, Germany: A new member of the autunite group. *Can. Mineral.* **2010**, *48*, 335–350. (In French) [CrossRef]
30. Plášil, J.; Cejka, J.; Sejkora, J.; Hloušek, J.; Goliáš, V. New data for metakirchheimerite from Jáchymov (St. Joachimsthal), Czech Republic. *J. Geosci.* **2009**, *54*, 373–384.
31. Plášil, J.; Sejkora, J.; Cejka, J.; Škácha, P.; Goliáš, V.; Ederová, J. Characterization of phosphate-rich metalodèvite from Príbram, Czech Republic. *Can. Mineral.* **2010**, *48*, 113–122. [CrossRef]
32. Locock, A.J.; Burns, P.C. The crystal structure of synthetic autunite, $Ca[(UO_2)(PO_4)]_2(H_2O)_{11}$. *Am. Mineral.* **2003**, *88*, 240–244. [CrossRef]
33. Sowder, A.G. Dehydration of synthetic autunite hydrates. *Radiochim. Acta* **2000**, *88*, 533–538. [CrossRef]
34. Makarov, E.S.; Ivanov, V.I. The crystal structure of meta-autunite, $Ca(UO_2)_2(PO4)_2.6H_2O$. *Doklady Akademii Nauk USSR* **1960**, *132*, 601–603.
35. Mrose, M.E. Studies of uranium minerals (XIII): Synthetic uranospinites. *Am. Mineral.* **1953**, *38*, 1159–1168.
36. Takano, Y. X-ray study of autunite. *Am. Mineral.* **1961**, *46*, 812–822.
37. Suzuki, Y.; Sato, T.; Isobe, H.; Kogure, T.; Murakami, T. Dehydration processes in the meta-autunite group minerals meta-autunite, metasaléeite, and metatorbernite. *Am. Mineral.* **2005**, *90*, 1308–1314. [CrossRef]
38. Lazić, B.; Kahlenberg, V.; Vulić, P.; Pešić, L.; Dimitrijević, R. Meta-autunite from a Li-pegmatite of the Cer Mt., Serbia: Its mineralogical and XRD investigations. *Neues Jahrb. Mineral. Abh.* **2009**, *186*, 333–344. [CrossRef]
39. Locock, A.J. Trends in actinides compounds with the autunite-sheet topology. *Zap. Vser. Mineral. Obshchest.* **2007**, *136*, 115–137.
40. Locock, A.J.; Burns, P.C.; Flynn, T.M. Structures of strontium- and barium-dominant compounds that contain the autunite-type sheet. *Can. Mineral.* **2005**, *43*, 721–733. [CrossRef]
41. Barinova, A.V.; Rastsvetaeva, R.K.; Sidorenko, G.A.; Chukanov, N.V.; Pushcharovskii, D.Y.; Pasero, M.; Merlino, S. Crystal structure of meta-uranocircite $Ba(UO_2)_2(PO_4)_2{\cdot}6H_2O$. *Dokl. Chem.* **2003**, *389*, 58–61. [CrossRef]
42. Dal Bo, F.; Hatert, F.; Baijot, M.; Philippo, S. Crystal structure of arsenuranospathite from Rabejac, Lodève, France. *Eur. J. Mineral.* **2015**, *27*, 589–597. [CrossRef]
43. Locock, A.J.; Kinman, W.S.; Burns, P.C. The structure and composition of uranospathite, $Al_{1-x}\square_x[(UO_2)(PO_4)]_2(H_2O)_{20+3x}F_{1-3x}$, $0 < x < 0.33$, a non-centrosymmetric fluorine-bearing mineral of the autunite group, and of a related synthetic lower hydrate, $Al_{0.67}\square_{0.33}[(UO_2)(PO_4)]_2(H_2O)_{15.5}$. *Can. Mineral.* **2005**, *43*, 989–1003.
44. Theye, T.; Walenta, K.; Markl, G. The chemical composition of uranospathite, arsenuranospathite, and associated minerals revisited the peculiarity of fluorine incorporation in autunite group minerals. *Neues Jahrb. Mineral. Abh.* **2016**, *193*, 59–68. [CrossRef]
45. Chukanov, N.V.; Möckel, S.; Sidorenko, G.A.; Zaitsev, V.A. Arsenuranospathite, $Al(UO_2)_2(AsO_4)_2F{\cdot}20H_2O$: Formula revision and relationships with allied uranyl arsenates and phosphates. *Neues Jahrb. Mineral. Abh.* **2009**, *185*, 305–312.
46. Walenta, K. Uranospathite and arsenuranospathite. *Mineral. Mag.* **1978**, *42*, 117–128. [CrossRef]
47. Belova, L.N.; Fedorov, O.V.; Lyubomilova, G.V.; Vishnev, A.I. Ferriferous umohoite. *Izv. Akad. Nauk SSSR Ser. Geol.* **1985**, *12*, 131–135.
48. Deliens, M.; Piret, P.; Comblain, G. *Les Minéraux Secondaires D'uranium Du Zaïre*; Musée royal de l'Afrique Centrale: Tervuren, Belgique, 1981; p. 113.

49. Krivovichev, S.V.; Burns, P.C. Crystal chemistry of uranyl molybdates. I. The structure and formula of umohoite. *Can. Mineral.* **2000**, *38*, 717–726. [CrossRef]
50. Deliens, M. Etude comparative des calcurmolites de Rabejac (Lodeve, Herault, France) et de l'Union Sovietique. *Ann. Soc. Geol. Belg.* **1992**, *115*, 91–97.
51. Rudnitskaya, L.S. Calcium uranium molybdate, $Ca(UO_2)_3(MoO_4)_3(OH)_2{\cdot}8H_2O$. In Proceedings of the Second International Conference on the Peaceful Uses of Atomic Energy, Geneva, Switzerland, 1–13 September 1958; p. 286.
52. Fedorov, O.V. The second finding of the calcium molybdate of uranium in the USSR. *Zapiski Vsesoyuznogo Mineralogicheskogo Obshchestva* **1963**, *92*, 464–465.
53. Sidorenko, G.A.; Chistyakova, N.I.; Chukanov, N.V.; Naumova, I.S.; Rassulov, V.A. Carcurmolite: New data on chemical composition and constitution the mineral. *New Data Miner.* **2005**, *40*, 29–36.
54. Finch, R.L.; Burns, P.C.; Hawthorne, F.C.; Ewing, R.C. Refinement of the crystal structure of billietite, $Ba[(UO_2)6O_4(OH)_6](H_2O)_8$. *Can. Mineral.* **2006**, *44*, 1197–1205. [CrossRef]
55. Piret-Meunier, J.; Piret, P. Nouvelle détermination de la structure cristalline de la bequerelite. *Bull. Minéral.* **1982**, *105*, 606–610.
56. Pagoaga, M.K.; Appleman, D.E.; Stewart, J.M. Crystal structures and crystal chemistry of the uranyl oxide hydrates becquerelite, billietite, and protasite. *Am. Mineral.* **1987**, *72*, 1230–1238.
57. Burns, P.C.; Li, Y. The structures of becquerelite and Sr-exchanged becquerelite. *Am. Mineral.* **2002**, *87*, 550–557. [CrossRef]
58. Mereiter, K. The crystal structure of liebigite, $Ca_2UO_2(CO_3)_3{\sim}11H_2O$. *Tschermaks Mineralogische und Petrographische Mitteilungen* **1982**, *30*, 277–288. [CrossRef]
59. Plášil, J.; Sejkora, J.; Ondruš, P.; Veselovský, F.; Beran, P.; Goliáš, V. Supergene minerals in the Horní Slavkov uranium ore district Czech Republic. *J. Geosci.* **2006**, *51*, 149–158. [CrossRef]
60. Capus, G. Matière Organiques et Minéralisations Uranifères, Exemples des Bassins Permo-Carbonifères de l'Aumance (Ailler) et de Lodève (Hérault). Ph.D. Thesis, École supérieure des sciences et technologies de l'ingénieur de Nancy, Vandœuvre-lès-Nancy, France, 1980. (In French)
61. Landais, P.; Connan, J. Relation uranium-matière organique dans deux bassins permiens français (Lodève-Hérault-Cérilly-Allier). *Bull. Cent. Rech. Explor. Prod. Elf-Aquitaine* **1980**, *4*, 709–757. (In French)
62. Mendez-Santizo, J. Approche Géothermique des Remplissages de Fractures Dans le Gisement D'uranium du Lodève. Ph.D Thesis, Université de Strasbourg, Strasbourg, France, 1986. (In French)
63. Nmila, A.; Cabanis, B.; Dardel, J.; Saint-Martin, J.; Treuil, M. Reliques volcaniques dans le remplissage permien du bassin de Lodève, incidences métallogéniques. *C. R. Acad. Sci. Paris* **1989**, *309*, 1931–1938.
64. Lancelot, J.R.; Saint-André, B.; de la Boisse, H. Systématique U–Pb et évolution du gisement d'uranium de Lodève (France). *Miner. Depos.* **1984**, *19*, 44–53. (In French) [CrossRef]
65. Frondel, C. Mineral composition of gummite. *Am. Mineral.* **1956**, *41*, 539–568.
66. Finch, R.J.; Ewing, R.C. The corrosion of uraninite under oxidizing conditions. *J. Nucl. Mater.* **1992**, *190*, 133–156. [CrossRef]
67. Plášil, J. Uranyl-oxide hydroxy-hydrate minerals their structural complexity and evolution trends. *Eur. J. Mineral.* **2017**, *30*, 1–15. [CrossRef]
68. Finch, R.J.; Murakami, T. Systematics and paragenesis of uranium minerals. In *Uranium: Mineralogy, Geochemistry and the Environment*; Burns, P.C., Finch, R., Eds.; De Gruyter: Berlin, Germany, 1999; pp. 91–179.
69. Plášil, J. Oxidation-hydration weathering of uraninite the current state-of-knowledge. *J. Geosci.* **2014**, *59*, 99–114. [CrossRef]
70. Sergeyeva, E.I.; Nikitin, A.A.; Khodakovsky, I.L.; Naumov, G.B.; Vernadskiy, V.I. Experimental investigation of equilibria in the system UO_3-CO_2-H_2O in 25–200 °C temperature intervals. *Geochem. Int.* **1972**, *11*, 900–910.
71. Deliens, M.; Piret, P. L'urancalcarite, $Ca(UO_2)_3CO_3(OH)6.3H_2O$, nouveau minéral de Shinkolobwe, Shaba, Zaïre. *Bull. Minéral.* **1984**, *107*, 21–24.
72. Krivovichev, S.V.; Plášil, J. Mineralogy and crystallography of uranium. In *Uranium–Cradle to Grave*; Burns, P.C., Sigmon, G.E., Eds.; Mineralogical Association of Canada: Québec, QC, Canada, 2013; pp. 15–119.